Published in final edited form as:
J Orthop Sci. 2011 May ; 16(3): 298–303. doi:10.1007/s00776-011-0051-5.

Differential fracture healing resulting from fixation stiffness variability: A mouse model

Michael J. Gardner, MD, **Sara Putnam, BS**, **Ambrose Wong, MD**, **Philipp N. Streubel, MD**, **Akhilesh Kotiya, PhD**, and **Matthew J. Silva, PhD**
Department of Orthopaedic Surgery, Washington University School of Medicine, St. Louis, MO

Abstract

Background—The mechanisms underlying the interaction between the local mechanical environment and fracture healing are not known. We developed a mouse femoral fracture model with implants of different stiffness, and hypothesized that differential fracture healing would result.

Methods—Femoral shaft fractures were created in 70 mice, and were treated with an intramedullary nail made of either tungsten (Young's modulus = 410 GPa) or aluminum (Young's modulus = 70 GPa). Mice were then sacrificed at two weeks or five weeks. Fracture calluses were analyzed using standard microCT, histological, and biomechanical methods.

Results—At two weeks, callus volume was significantly greater in the aluminum group compared to the tungsten group (61.2 mm^3 vs 40.5 mm^3; p = 0.016), yet bone volume within the calluses was no different between the groups (13.2 mm^3 vs 12.3 mm^3). Calluses from the tungsten group were more stiff on mechanical testing (18.7 N/mm vs 9.7 N/mm, p = 0.01). The percent cartilage in the callus was 31.6% in the aluminum group and 22.9% in the tungsten group (p = 0.40). At 5 weeks, there were no differences between any of the healed femora.

Conclusions—In this study, fracture implants with different stiffnesses led to differential fracture healing in this mouse fracture model. Fractures treated with a stiffer implant had more advanced healing at two weeks, but still healed by callus formation. Although this concept has been well documented previously, this particular model could provide a valuable research tool to study the healing consequences of altered fixation stiffness, which may provide insight into the pathogenesis and ideal treatment of fractures and nonunions.

Introduction

Despite the recent refinement of surgical fracture treatment techniques, many fractures do not achieve timely union. Depending on the fracture pattern, associated comminution, and anatomical region, surgical treatment aims for either rigid fixation, with direct remodeling, or flexible fixation, with healing by secondary callus formation. In the latter, the magnitude and rate of callus formation depends directly on fixation construct stiffness.[1, 2]

Fracture fixation stiffness equates to fracture site motion under a given physiologic load. Optimal callus formation results when fracture motion is within a specific range; if the motion is outside of this range, either too low or too high, fracture healing is impaired.[3] Because of the complexities of the multiple codependent molecular pathways in the fracture

Correspondence to: Michael J. Gardner, MD, Washington University School of Medicine, Department of Orthopaedic Surgery, 660 S. Euclid Ave, Campus Box 8233, St. Louis MO, 63110, Phone: (314)747-2523, Fax: (314)747-2599, gardnerm@wudosis.wustl.edu.

Financial disclosure: MJG is a consultant for Synthes, Amgen, and DGIMed. No outside funding was received in support of this work.

healing cascade, the precise mechanisms by which fracture site motion affects callus formation are unknown.

Elucidation of the pathways involved in this process is vital to improving the clinical care of fractures. Aside from advancing the understanding of the pathogenesis of nonunion formation, this may also lead to focused exogenous interventions using recombinant proteins to augment fracture healing. Much of the previous work on fracture site motion and fracture healing has been performed using large animal models.[3–5] These models have necessarily used small numbers of specimens, and have not allowed for the genetic and molecular analyses of fracture healing that are currently possible in murine models.

Previous investigators have adapted mouse femur internal fixation devices with the goal of creating absolute rigidity to study the associated molecular events.[6–9] However, a model that allows for variations in fixation stiffness, all within the range that allows for callus formation, may provide insight into the subtle molecular differences that are important to the link between the mechanical environment and callus formation. We hypothesized that using intramedullary nails of different stiffnesses would lead to variations in fracture healing.

Materials and Methods

After study design approval from the institutional Animal Studies Committee, closed unilateral femoral shaft fractures were created in 70 male ten-week old C57Bl/J6 wild type mice. Mice were randomly assigned to receive a femoral nail made of either tungsten or aluminum. Tungsten (Tu) has a relatively high Young's modulus (410 GPa) and aluminum (Al) has a low modulus (70 GPa). Following induction of general anesthesia by intraperitoneal injection of a xylazine/ketamine cocktail, the right hindlimb was shaved and sterilely prepared. An incision was made over the distal femur. The patella was subluxated to expose the femoral condyles, and the intercondylar notch was opened with a 25 Gauge needle. The selected wire was 0.5 mm in diameter, and was cut to the appropriate length. The ends were flattened with pliers to establish an intramedullary interference fit, and the nail was inserted until it was fully seated. The incision was irrigated and closed with sutures.

Following nail insertion, a closed fracture was created using a well described three-point bending device.[10] Faxitron radiographs were used to confirm fracture creation and accurate implant placement. Mice were then given a buprenorphine injection for postoperative pain control, and were awakened and allowed unrestricted cage activity. Mice in each fixation group were randomly assigned to be sacrificed at 2 or 5 weeks. These time points correspond to early and later (after callus remodeling) stages of fracture healing, respectively.[11] After sacrifice by carbon dioxide inhalation, the operated hindlimbs were dissected free of soft tissues, and the intramedullary nails were removed. The specimens were then wrapped in moist gauze and stored at −20° C prior to analysis.

Fracture calluses were analyzed using several methods. First, plain radiographs of all harvested specimens were obtained (Faxitron MX-20) and analyzed by three independent investigators. A subset of the Goldberg scale[12] was applied to determine healing (0 = no union; 1 = partial union; 2 = definite complete union). Two investigators blindly graded radiographic healing, and any discrepancies were adjudicated by a third investigator. Second, microCT was performed to quantify callus volume, bone volume, and mineral density (n = 9–11 per group). Specimens were embedded in 1% agarose and placed in a 16.4 mm diameter tube and scanned over their entire lengths using a desktop microCT system (μCT40 Scanco Medical AG, Bassersdorf, Switzerland). Scan settings were as follows: voxel size 16 um, standard resolution, 55 kVp, 147 μA, and integration time 300 ms. Images were filtered (gauss sigma 1.2) and a three-dimensional reconstruction was performed, from

which the center of the fracture location was visually identified. A volume spanning 300 slices (4.8 mm), 150 slices above and below the fracture, was then analyzed. Contours marking the outer margin of the callus were drawn. A global threshold of 250 (on a grayscale of 0–1000) was applied to segment bone from non-bone. The following parameters were computed: total callus volume (TV, mm^3), total bone volume (BV, mm^3), bone volume fraction (BV/TV), volumetric bone mineral density of total callus volume (BMD), and tissue mineral density of bone (TMD).

The third method for analysis of the callus was histological (n = 5 per group). The bones were fixed for 24 hours in 4% paraformaldehyde solution. Specimens were decalcified in 14% EDTA solution for 2 weeks, dehydrated in progressive concentrations of ethanol, and embedded in paraffin. Bone samples were progressively sectioned sagitally until a slice was obtained that best contained all four cortices of the original fracture site. Longitudinal sections were stained with picosirius red and alcian blue. Sections were analyzed using the freeware ImageJ v1.42q (http://rsb.info.nig.gov/ij). Contours were manually drawn around the callus perimeter. Medullary space was excluded from calculations for total callus area, as well as from any calculations involving total cartilage area within the callus. In an effort to reduce variability that may have been introduced by manually creating the contours, the callus was blindly outlined three times, and total callus area and cartilage area were derived from averages of the three individual manual tracings for each specimen. Calculated parameters included total cartilage area and percent cartilage area (cartilage area/total callus area).

Intact and fractured specimens (n = 8 per group) then underwent biomechanical testing using a materials testing system (Instron 8841). Just prior to testing, the femurs were thawed at 20° C and soaked in PBS for 20 minutes. Each bone was placed on two supports spaced 7 mm apart and a transverse force was applied at the mid-diaphysis under displacement control (0.03 mm/s) until fracture. Force and displacement data were collected at 60 Hz (Labview, National Instruments). From force-displacement plots we determined: stiffness, yield force, ultimate force, post-yield displacement and energy to fracture.

The radiographic healing assessment based on the Goldberg scale was compared between each group at each time point using Fisher's exact tests. We calculated the mean and standard deviations for multiple parameters of biomechanical testing, microCT, and histology. For the biomechanical test results, each group was compared to its contralateral control specimen at both 2 and 5 weeks, and the experimental groups were compared to each other at each time point using two-tailed Student's t-tests. For microCT and histology, the experimental groups were compared, also using Student's t-tests. All analyses were performed using a commercial statistical software package (SPSS v. 11.0, SPSS, Inc, Chicago, IL).

Results

At two weeks, multiple differences were found between the aluminum and tungsten groups. All femora were radiographically healed by the Goldberg scale criteria in the tungsten group, whereas two specimens remained nonunited in the aluminum group (Figure 1). Overall, the incidence of healing did not differ between groups (p = 0.48). On microCT, total callus volume (TV) in the Al group was significantly larger than in the Tu group (61.2 vs. 40.5; p = 0.016). Despite the larger callus volumes, bone volume (BV) in the Al group was no different than in the Tu group at two weeks (13.2 vs. 12.3 mm^3, Figure 2). Accordingly, the BV/TV ratio was significantly lower in the aluminum group (22.2 vs. 32.6%; p = 0.027,). This indicates that the calluses in the bones fixed with an aluminum nail were larger in size, but contained a similar amount of bone tissue compared to bones fixed

the more stiff tungsten nail. On histological analysis, fracture healing proceeded via endochondral ossification in both the aluminum and tungsten groups. The aluminum group calluses contained 32% cartilage, compared to 23% in the tungsten group, although this difference was not significant ($p = 0.44$; Figure 3).

At two weeks, both the tungsten and aluminum fracture groups had significantly inferior biomechanical properties lower bending stiffness compared to their contralateral control specimens, indicating incomplete restoration of mechanical competence at this early time point (Table 1). Femora from the aluminum group had a two-fold lower stiffness than those from the tungsten group (9.7 vs 18.7 N/mm, $p = 0.01$, Table 1). However, femora from the aluminum group had a significantly greater post-yield displacement (i.e., the amount of displacement between the onset of initial failure and final failure) compared to the tungsten group (1.05 vs. 0.54 mm, $p < 0.002$, Table 1). This indicates a more ductile callus in the aluminum group. Because the aluminum calluses were larger, less stiff, and required more displacement to yield, the total area under the force-displacement curve (energy to fracture) was also greater in these specimens (6.28 vs 3.42 N*mm, $p = 0.02$, Table 1). There were no differences in yield force or post-yield displacement between the groups.

At 5 weeks, all fractures were fully healed radiographically, and no cartilage was evident on the histological sections. No differences in biomechanical parameters or microCT analysis were found at 5 weeks between the groups (Table 2).

Discussion

Fracture union after surgical stabilization is not inevitable, and depends on multiple factors. A predominant variable is the fracture implant stiffness, which directly affects fracture site motion. Within the appropriate range of fracture motion, effective callus forms and the fracture unites.[3] The mechanisms by which fracture motion and callus formation are linked are unknown, and necessitate further study. Mouse fracture models have become invaluable for studying the molecular aspects of fracture healing, given the interspecies similarities between murine and human pathways.[8, 13–16] Additionally, murine models provide the potential for genetic manipulations to study specific factors and pathways.[17, 18] In this study, we developed a novel mouse fracture model which employed variable stiffness fixation, in an attempt to achieve differential healing responses. Our hypothesis was confirmed, in that the different fixation stiffnesses led to variations in fracture healing progress. This was evident by the larger calluses in the less stiff aluminum fixation group. Interestingly, despite the larger overall callus volume, the aluminum group calluses contained similar amounts of bone as the tungsten calluses, resulting in lower callus bone density. This also led to mechanically inferior calluses in the aluminum group at two weeks, with significantly lower stiffness and greater post-yield displacement. The direct relationship between fracture site motion and healing progress has been clearly demonstrated previously and is well accepted. The current mouse model using different implant stiffnesses is sufficiently sensitive to demonstrate this differential phenomenon, and may be valuable in studying the molecular events underlying this process.

It is not clear from this study whether fracture healing pathways were different between the groups, or whether the time course of fracture healing was delayed in the aluminum group. Several mechanistic possibilities are plausible. The actual fracture site motion was unable to be quantified *in vivo*, given the small size of murine femora. However, given the fractures and postoperative protocols were identical between the groups, the only factor that determined fracture motion was the bending stiffness of the implants, which was 80% lower for the aluminum rods compared to the tungsten rods. Thus it can be confidently presumed that the aluminum implant allowed for greater motion. The physiologic response to this

increased motion is to increase the diameter of the callus (and the cross-sectional moment of inertia), perhaps to the point where the strain at the peripheral callus tissue is reduced to a level point that is within the tissue tolerance for bone formation.[19, 20] Thus, based on the these principles, the aluminum group may have demonstrated an exaggerated callus response to accommodate for this greater fracture site motion.

Alternatively, it has previously been postulated that angiogenesis is affected by fracture site motion.[21, 22] A fracture immediately severs the majority of perfusing vasculature, leading to a local hypoxic environment and low oxygen tension.[23] Cells within the hematoma and early granulation tissue at the center of the fracture zone must differentiate and proliferate in an anaerobic state, and require eventual vascular ingrowth to proceed to endochondral ossification.[24] Fragile developing capillary buds may be particularly susceptible to mechanical perturbation, such as with increased fracture site motion from relatively flexible fracture fixation. Thus, the increased fracture site motion in the aluminum group may have resulted in relative persistence of the hypoxic state, leading to a delay in union. This is consistent with the smaller, more mature calluses in the tungsten group, as well as the significantly greater stiffness found on mechanical testing. Additional studies are needed to address this issue. Other theories regarding the effects of fracture site motion on callus formation include cell deformation causing changes in membrane permeability, fluid flow, and biological activity.[25, 26]

A main limitation of this study is the relatively few time points studied. Of the two time points evaluated, the 5 week interval predictably demonstrated full fracture healing in both fixation groups, with no detectable differences on any of the outcome measures. This confirmed that both implants were suitable to allow fracture healing to eventually occur. The two week time point was chosen as a an early interval during the healing process, but prior to complete remodeling. Significant differences were found between the groups at this point, but to further characterize the time course of healing with each implant, additional time points, both before and after 2 weeks are necessary. Also, no analyses were performed in this study to allow us to hypothesize on the reasons for variable fracture healing between the groups, and this is also a topic for further study.

Elucidation of the specific pathways involved in the coupling of the local mechanical environment to callus formation is vital to improve upon current fracture healing interventions. Our data indicate that this variable stiffness model provides a means to study specific fracture healing pathways, and their relative role related to fracture site motion. Exogenous and targeted recombinant protein applications may eventually provide an adjunct to nonunion treatment. Specifically, fracture fixation constructs are often applied in such a fashion to optimize fixation strength to minimize fixation failure risk, but at the expense of an overly stiff implant. This may lead to minimal fracture site motion, early regional normoxia, downregulation of angiogenic or other critical factors, and inadequate biological activity to successfully heal the fracture. Additionally, future research may allow insight into the optimal fracture fixation construct stiffness in various clinical circumstances.

Acknowledgments

We thank Tarpit Patel, M.S., for assistance with microCT analysis and mechanical testing, which were supported in part by NIH/NIAMS grants P30AR057235 (Washington University Core Center for Musculoskeletal Biology and Medicine).

References

1. Uhthoff HK, Finnegan MA. The role of rigidity in fracture fixation. An overview. Arch Orthop Trauma Surg. 1984; 102:163–6. [PubMed: 6703873]

2. Kenwright J, Gardner T. Mechanical influences on tibial fracture healing. Clin Orthop. 1998; 355(Suppl):S179–90. [PubMed: 9917638]

3. Epari DR, Kassi JP, Schell H, Duda GN. Timely fracture-healing requires optimization of axial fixation stability. J Bone Joint Surg Am. 2007; 89:1575–85. [PubMed: 17606797]

4. Claes L, Eckert-Hubner K, Augat P. The fracture gap size influences the local vascularization and tissue differentiation in callus healing. Langenbecks Arch Surg. 2003; 388:316–22. [PubMed: 13680236]

5. Augat P, Burger J, Schorlemmer S, Henke T, Peraus M, Claes L. Shear movement at the fracture site delays healing in a diaphyseal fracture model. J Orthop Res. 2003; 21:1011–7. [PubMed: 14554213]

6. Histing T, Holstein JH, Garcia P, Matthys R, Kristen A, Claes L, Menger MD, Pohlemann T. Ex vivo analysis of rotational stiffness of different osteosynthesis techniques in mouse femur fracture. J Orthop Res. 2009; 27:1152–6. [PubMed: 19215028]

7. Garcia P, Holstein JH, Histing T, Burkhardt M, Culemann U, Pizanis A, Wirbel RJ, Pohlemann T, Menger MD. A new technique for internal fixation of femoral fractures in mice: impact of stability on fracture healing. J Biomech. 2008; 41:1689–96. [PubMed: 18462739]

8. Holstein JH, Garcia P, Histing T, Kristen A, Scheuer C, Menger MD, Pohlemann T. Advances in the establishment of defined mouse models for the study of fracture healing and bone regeneration. J Orthop Trauma. 2009; 23:S31–8. [PubMed: 19390374]

9. Holstein JH, Menger MD, Culemann U, Meier C, Pohlemann T. Development of a locking femur nail for mice. J Biomech. 2007; 40:215–9. [PubMed: 16376352]

10. Bonnarens F, Einhorn TA. Production of a standard closed fracture in laboratory animal bone. J Orthop Res. 1984; 2:97–101. [PubMed: 6491805]

11. Manigrasso MB, O'Connor JP. Characterization of a closed femur fracture model in mice. J Orthop Trauma. 2004; 18:687–95. [PubMed: 15507822]

12. Goldberg VM, Powell A, Shaffer JW, Zika J, Bos GD, Heiple KG. Bone grafting: role of histocompatibility in transplantation. J Orthop Res. 1985; 3:389–404. [PubMed: 3906062]

13. Shen X, Wan C, Ramaswamy G, Mavalli M, Wang Y, Duvall CL, Deng LF, Guldberg RE, Eberhart A, Clemens TL, Gilbert SR. Prolyl hydroxylase inhibitors increase neoangiogenesis and callus formation following femur fracture in mice. J Orthop Res. 2009; 27:1298–305. [PubMed: 19338032]

14. Gardner MJ, van der Meulen MC, Carson J, Zelken J, Ricciardi BF, Wright TM, Lane JM, Bostrom MP. Role of parathyroid hormone in the mechanosensitivity of fracture healing. J Orthop Res. 2007; 25:1474–80. [PubMed: 17568439]

15. Ogasawara A, Nakajima A, Nakajima F, Goto K, Yamazaki M. Molecular basis for affected cartilage formation and bone union in fracture healing of the streptozotocin-induced diabetic rat. Bone. 2008; 43:832–9. [PubMed: 18725334]

16. Palomares KT, Gleason RE, Mason ZD, Cullinane DM, Einhorn TA, Gerstenfeld LC, Morgan EF. Mechanical stimulation alters tissue differentiation and molecular expression during bone healing. J Orthop Res. 2009; 27:1123–32. [PubMed: 19242967]

17. Shomento SH, Wan C, Cao X, Faugere MC, Bouxsein ML, Clemens TL, Riddle RC. Hypoxia-inducible factors 1alpha and 2alpha exert both distinct and overlapping functions in long bone development. J Cell Biochem. 2010; 109:196–204. [PubMed: 19899108]

18. Rundle CH, Wang X, Wergedal JE, Mohan S, Lau KH. Fracture healing in mice deficient in plasminogen activator inhibitor-1. Calcif Tissue Int. 2008; 83:276–84. [PubMed: 18820962]

19. Augat P, Simon U, Liedert A, Claes L. Mechanics and mechano-biology of fracture healing in normal and osteoporotic bone. Osteoporos Int. 2005; 16(Suppl 2):S36–43. [PubMed: 15372141]

20. Perren SM. Evolution of the internal fixation of long bone fractures. The scientific basis of biological internal fixation: choosing a new balance between stability and biology. J Bone Joint Surg Br. 2002; 84:1093–110. [PubMed: 12463652]

21. Lienau J, Schell H, Duda GN, Seebeck P, Muchow S, Bail HJ. Initial vascularization and tissue differentiation are influenced by fixation stability. J Orthop Res. 2005; 23:639–45. [PubMed: 15885486]

22. Glowacki J. Angiogenesis in fracture repair. Clin Orthop Relat Res. 1998:S82–9. [PubMed: 9917629]

23. Brighton CT, Krebs AG. Oxygen tension of healing fractures in the rabbit. J Bone Joint Surg Am. 1972; 54:323–32. [PubMed: 4651264]

24. Gerstenfeld LC, Cullinane DM, Barnes GL, Graves DT, Einhorn TA. Fracture healing as a post-natal developmental process: molecular, spatial, and temporal aspects of its regulation. J Cell Biochem. 2003; 88:873–84. [PubMed: 12616527]

25. Allen FD, Hung CT, Pollack SR, Brighton CT. Serum modulates the intracellular calcium response of primary cultured bone cells to shear flow. J Biomech. 2000; 33:1585–91. [PubMed: 11006382]

26. Pavalko FM, Norvell SM, Burr DB, Turner CH, Duncan RL, Bidwell JP. A model for mechanotransduction in bone cells: the load-bearing mechanosomes. J Cell Biochem. 2003; 88:104–12. [PubMed: 12461779]

Figure 1.
Radiograph examples of the aluminum group at 2 weeks (A) and 5 weeks (B), and the tungsten group at 2 weeks (C) and 5 weeks (D).

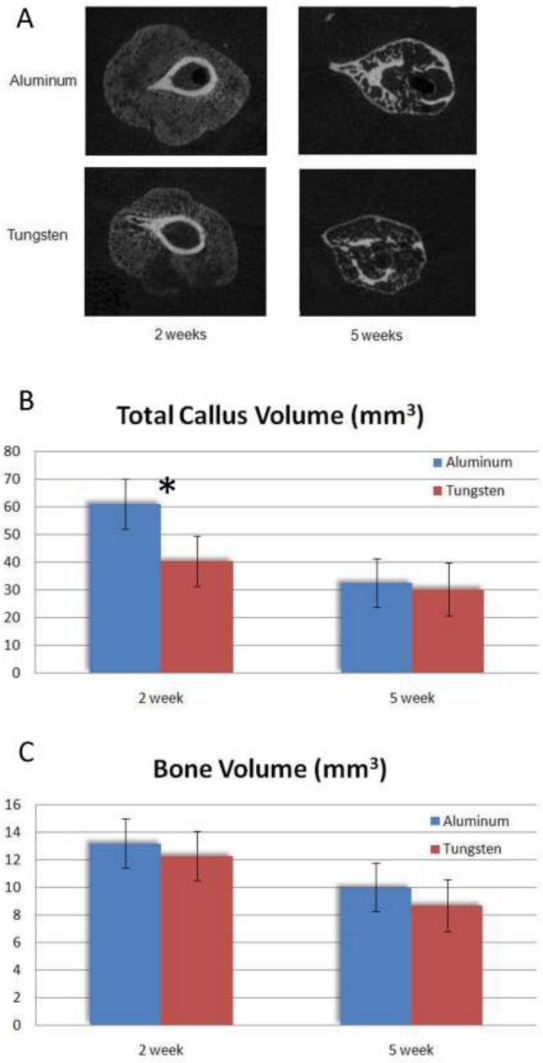

Figure 2.
Examples of cross-sectional microCT's of each group at both time points (A). The total callus volume of the aluminum group was greater (*, $p < 0.05$) than the tungsten group (B). Despite this, callus bone volume was no different between the groups at two weeks (C).

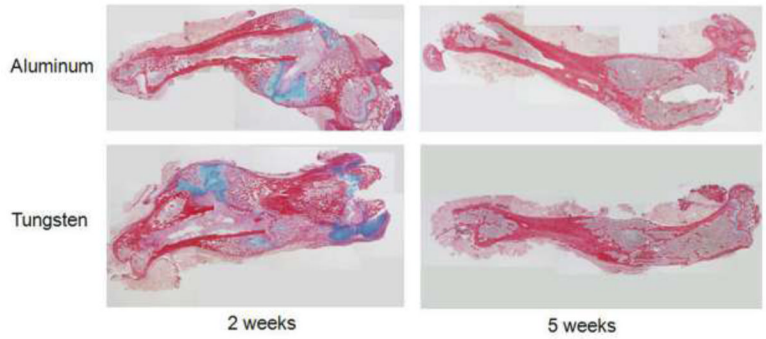

Figure 3.
Representative histology sections from each group at 2 and 5 weeks. At 2 weeks, there was a non-significant trend for more cartilage per callus area in the Aluminum specimens (32 vs 23%).

Table 1

Biomechanical comparisons between the groups at 2 weeks post-fracture.

	Aluminum	Control	p	Tungsten	Control	p	Aluminum	Tungsten	p
Yield Force (N)	7.54	13.20	0.00	7.57	15.11	0.00	7.54	7.57	0.98
Ultimate Force (N)	8.79	17.43	0.00	8.61	18.86	0.00	8.79	8.61	0.91
Stiffness (N/mm)	9.68	69.66	0.00	18.69	71.59	0.00	9.68	18.69	0.01
Post-yield Displacement (mm)	0.40	1.05	0.00	0.18	0.79	0.02	0.40	0.18	0.20
Energy at Fracture Force (N*mm)	6.28	13.78	0.00	3.42	12.13	0.00	6.28	3.42	0.02

Table 2

Biomechanical comparisons between the groups at 5 weeks post-fracture.

	Aluminum	Control	p	Tungsten	Control	p	Aluminum	Tungsten	P
Yield Force (N)	17.79	17.89	0.98	14.67	18.36	0.12	17.79	14.67	0.42
Ultimate Force (N)	19.72	20.02	0.94	17.47	20.54	0.13	19.72	17.47	0.58
Stiffness (N/mm)	50.29	60.35	0.62	51.15	71.00	0.19	50.29	51.15	0.96
Post-yield Displacement (mm)	0.16	0.66	0.06	0.29	0.65	0.01	0.16	0.29	0.25
Energy at Fracture Force (N*mm)	7.34	11.38	0.11	7.36	12.93	0.01	7.34	7.36	0.99